Relaxation-induced polarized luminescence from $In_xGa_{1-x}As$ films grown on GaAs(001)

K. Rammohan, Y. Tang, and D. H. Rich*
Photonic Materials and Devices Laboratory, Department of Materials Science and Engineering, University of Southern California, Los Angeles, California 90089-0241

R. S. Goldman, H. H. Wieder, and K. L. Kavanagh
Department of Electrical and Computer Engineering, University of California, San Diego, La Jolla, California 92093-0407
(Received 22 August 1994; revised manuscript received 14 November 1994)

We have investigated local variations in the optical properties of $In_{0.06}Ga_{0.94}As/GaAs$ using linearly polarized cathodoluminescence imaging and spectroscopy. The influence of substrate misorientation on the polarization anisotropy of excitonic luminescence in the $In_{0.06}Ga_{0.94}As$ films was examined. Local variations in excitonic polarization anisotropy and emission energy are found to correlate spatially with dark line defects which result from the formation of interfacial misfit dislocations.

I. INTRODUCTION

Strain relaxation in lattice-mismatched semiconductor epilayers occurs by the formation of misfit dislocations. In the zinc-blende lattice, orthogonal $\langle 110 \rangle$ misfit dislocations (α,β) are not equivalent and generally possess different glide velocities and nucleation rates that affect the uniformity of strain relaxation.[1-5] Anisotropic electrical properties of these materials that have been observed along the orthogonal $\langle 110 \rangle$ direction,[6-9] have been attributed to the asymmetric strain relaxation caused by an anisotropic distribution of misfit dislocations. Also, the presence of misfit dislocations is known to degrade optical and electrical properties by introducing nonradiative recombination centers. Optical studies, utilizing luminescence imaging, have examined strain relaxation and its accompanying asymmetry in $In_xGa_{1-x}As/GaAs$ by measuring the density of dark line defects (DLD's).[10-12] In addition to influencing the local carrier recombination rate, the fluctuation in strain fields associated with misfit dislocation should influence the energy of the $In_xGa_{1-x}As$ excitonic luminescence and induce polarization effects.

In this paper, we demonstrate that strain relaxation in $In_xGa_{1-x}As$ films grown on GaAs correlates with local variations in the band gap and polarization of excitonic emission. The polarization effects are studied for two $In_{0.06}Ga_{0.94}As/GaAs(001)$ samples, which exhibit different degrees of anisotropic strain relaxation. The extent of the asymmetry in misfit dislocations formed during strain relaxation of $In_xGa_{1-x}As/GaAs(001)$ interfaces was found to be influenced by the geometry of the substrate misorientation.[12,13] In this study, we have investigated the effect of substrate misorientation on the asymmetric strain relaxation with cathodoluminescence (CL) imaging and spectroscopy. We have utilized an approach, in which a combination of linearly polarized CL (LPCL) (Refs. 14 and 15) and CL wavelength imaging (CLWI) (Ref. 16) is used to assess the spatial variations in the stress tensor of the $In_xGa_{1-x}As$ films. Polarization selection rules for excitonic emission in semiconductors depend on the form of stress tensor;[17] CLWI enables a mapping of the defect-, strain-, and composition-induced band-gap changes on the scale of ~ 1 μm, as the resolution is limited by the minority-carrier diffusion.

II. EXPERIMENTAL DETAILS

Samples were grown by solid source molecular-beam epitaxy. Details of the preparation and structural characterization have been described elsewhere.[12] They consisted of 280-nm-Si-doped ($N_d \approx 10^{17}$ cm^{-3}) $In_{0.06}Ga_{0.94}As$ on 500-nm-undoped GaAs buffers grown simultaneously on semi-insulating (001)-oriented GaAs substrates (a) nominally flat ($\pm 0.05°$) and (b) misoriented $2 \pm 0.05°$ towards the nearest (011) plane.

X-ray rocking curve (XRC) measurements showed that the sample grown on the nominally flat substrate relaxed 13 ± 1 and 12 ± 1 % in the [110] and [$1\bar{1}0$] directions, respectively, isotropic relaxation to within experimental error. The sample grown on the misoriented substrate relaxed 8 ± 1 and 20 ± 1 % in the [110] and [$1\bar{1}0$] directions, respectively, resulting in a distinct anisotropy. The average relaxation in the $In_xGa_{1-x}As$ film on the misoriented sample (14 ± 1 %) is only slightly larger than that on the flat substrate (12.5 ± 1%). From the x-ray results, estimates of the misfit dislocation density in each $\langle 110 \rangle$ direction were calculated assuming only 60° dislocations were present.[3] Thus, the estimated average dislocation density in the nominally flat sample was $2.5 \pm 0.1 \times 10^4$ cm^{-1} along both $\langle 110 \rangle$ directions. For the case of the misoriented sample, the estimated dislocation densities were 1.8 ± 0.1 and $4.5 \pm 0.2 \times 10^4$ cm^{-1} in the [110] and [$1\bar{1}0$] directions, respectively.

Scanning monochromatic CL, CLWI, and LPCL were performed with a modified JEOL 840-A scanning electron microscope.[14] A rotatable linear polarizer was mounted in vacuo to perform polarized measurements. The light collected was dispersed by a 0.25-m monochromator and detected with a cooled Cs:GaAs photomultiplier tube. An electron beam with a 15-keV beam energy was used to probe the sample, which was cooled to 87 K.

III. THEORY

The strain-induced splitting of the heavy-hole (hh; $m_j=\pm\frac{3}{2}$) and light-hole (lh; $m_j=\pm\frac{1}{2}$) valence bands at $\mathbf{k}=0$ can be examined by studying the polarization and energy dependence of the luminescence.[14,15,17] For a general biaxial stress (σ) in the (001) plane, which contains two orthogonal stress components $\sigma_\parallel$ and $\sigma_\perp$ (as referred to [110]), a diagonalization of the orbital-strain Hamiltonian enables a determination of the set of uppermost $J=\frac{3}{2}$ strain-split valence-band wave functions, u_i.[17] In the [110] representation of $|J,m_j\rangle$, these normalized wave functions are given by

$$u_i=c_{i,\mathrm{hh}}\left|\tfrac{3}{2},\tfrac{3}{2}\right\rangle_{110}+c_{i,\mathrm{lh}}\left|\tfrac{3}{2},-\tfrac{1}{2}\right\rangle_{110}, \tag{1}$$

where $i=1$ and 2 represent the highest and lowest bands, respectively. The coefficients $c_{i,\mathrm{hh}}$ and $c_{i,\mathrm{lh}}$ are given by

$$\begin{aligned} c_{1,\mathrm{hh}}&=-\frac{\eta}{\{\eta^2+[(\eta^2+\zeta^2)^{1/2}-\zeta]^2\}^{1/2}},\\ c_{1,\mathrm{lh}}&=\frac{(\eta^2+\zeta^2)^{1/2}-\zeta}{\{\eta^2+[(\eta^2+\zeta^2)^{1/2}-\zeta]^2\}^{1/2}},\\ c_{2,\mathrm{hh}}&=c_{1,\mathrm{lh}},\quad c_{2,\mathrm{lh}}=c_{1,\mathrm{hh}}, \end{aligned} \tag{2}$$

where the parameters η and ζ are represented in terms of the elastic compliance constants S_{11}, S_{12}, and S_{44}, the uniaxial deformation potentials b and d, and the in-plane stress components $\sigma_\parallel$ and $\sigma_\perp$:

$$\begin{aligned} \eta&=\frac{\sqrt{3}}{4}b(S_{11}-S_{12})\left[1+\frac{\sigma_\perp}{\sigma_\parallel}\right]-\frac{d}{8}S_{44}\left[1-\frac{\sigma_\perp}{\sigma_\parallel}\right],\\ \zeta&=\frac{b}{4}(S_{11}-S_{12})\left[1+\frac{\sigma_\perp}{\sigma_\parallel}\right]+\frac{\sqrt{3}}{8}dS_{44}\left[1-\frac{\sigma_\perp}{\sigma_{11}}\right] \end{aligned} \tag{3}$$

The elastic compliance constants and deformation potentials for $In_xGa_{1-x}As$ are approximated well by interpolating between the corresponding values for pure GaAs and InAs; these constants are given by $b=-1.7-0.1x$, $d=-4.55+0.95x$ (in eV), and $S_{11}=(1.176+0.769x)10^{-12}$, $S_{12}=(-0.365-0.32x)10^{-12}$, and $S_{44}=(1.684+0.841x)10^{-12}$ (in $\mathrm{cm^2/dyn}$), where $x=0.06$ in this study.[18–20]

Interband optical transitions involving the hh and lh states exhibit polarization selection rules which depend on the strain tensor, deformation potentials, and orientation of the electric field, $\mathbf{E}$, of light emitted or absorbed.[17] For a [110]-oriented pure uniaxial compressive stress (i.e., $\sigma_\perp=0$), very little mixing of the hh and lh bands occurs, as Eq. (2) yields $c_{1,\mathrm{hh}}=0.045$, when $\sigma_\perp=0$. The excitonic emission associated with the lh valence band is the lowest-energy transition and is partially linearly polarized parallel to [110]. The ratio of oscillator strengths of luminescence with $\mathbf{E}_\perp[110]$ polarization to that with $\mathbf{E}\|[110]$, $I_\perp/I_\parallel$, for the lowest-energy transition in the strain split bands is given by

$$\frac{I_\perp}{I_\parallel}=\frac{1}{4}\left[\sqrt{3}\frac{c_{1,\mathrm{hh}}}{c_{1,lh}}+1\right]^2, \tag{4}$$

where the calculation uses the dipole approximation in Fermi's golden rule, i.e., $I_{\perp,\parallel}\propto|\langle u_c|\mathbf{E}_{\perp,\parallel}\cdot\mathbf{p}|u_1\rangle|^2$, where u_c is the conduction-band wave function and $\mathbf{p}$ is the linear momentum operator. For pure uniaxial stress ($\sigma_\perp=0$) the calculated value of $I_\perp/I_\parallel$ is 0.29. We note that for a material in which there is no mixing of hh and lh characters in the valence bands ($c_{1,\mathrm{lh}}=1$ and $c_{1,\mathrm{hh}}=0$), Eq. (4) yields ideally $I_\perp/I_\parallel=\frac{1}{4}$. The calculated values for $I_\perp/I_\parallel$, $|c_{1,\mathrm{hh}}|^2$, and $|c_{1,\mathrm{lh}}|^2$ versus $\sigma_\perp/\sigma_\parallel$ in the [110] representation are shown in Fig. 1. For an in-plane biaxial compressive stress with $\sigma_\parallel=\sigma_\perp$, no polarization of the hh or lh excitonic emissions is expected as seen in Fig. 1, and the valence band associated with the lowest optical transition energy has a pure hh character when the wave functions are transformed to the [001] representation.

IV. RESULTS AND DISCUSSION

Figure 2 shows spatially averaged LPCL spectra of the bulk $In_{0.06}Ga_{0.94}As$ excitonic luminescence obtained from both samples. The electron beam was rastered over a 128×94 μm^2 region during acquisition. These spectra were taken with the polarizer rotated to detect emission of light with $\mathbf{E}\perp[110]$ and $\mathbf{E}\|[110]$ detection orientations. It is evident from both spectra that the misoriented substrate exhibits a greater degree of polarization anisotropy as compared to the flat substrate. The values of $I_\perp/I_\parallel$ are 0.926 and 0.877 for the sample grown on the flat and the misoriented substrate, respectively, where I is the integrated intensity and the subscript refers to its electric-field orientation.

The increased deviation of $I_\perp/I_\parallel$ from unity for the sample grown on the misoriented substrate as compared to the sample grown on the flat substrate is indicative of the greater level of anisotropic strain relaxation associated with the misorientation. Further, the luminescence intensity is highest when $\mathbf{E}\|[110]$, which indicates the presence of quasiuniaxial compressive stress along the [110] direction. This also corresponds to a greater relaxation along the $[1\bar{1}0]$ direction, which is in agreement with the

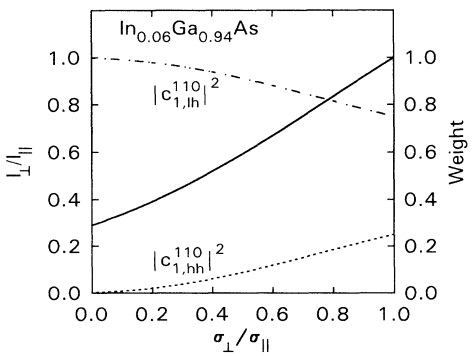

FIG. 1. Calculated intensity ratio ($I_\perp/I_\parallel$) of luminescence with $\mathbf{E}\perp[110]$ polarization to that with $\mathbf{E}\|[110]$, $|c_{1,\mathrm{hh}}^{110}|^2$, and $|c_{1,\mathrm{hh}}^{110}|^2$ versus $\sigma_\perp/\sigma_\parallel$ for $In_{0.06}Ga_{0.94}As$. The 110 superscripts are used to emphasize that the $|J,m_j\rangle$ basis wave functions are in the [110] representation here. The $\parallel$ and $\perp$ subscripts denote parallel and perpendicular to the [110] direction, respectively.

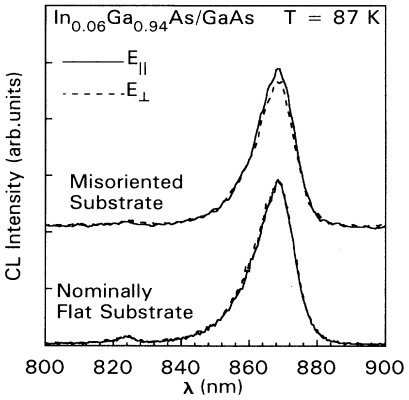

FIG. 2. Spatially averaged polarized CL spectra obtained for $In_{0.06}Ga_{0.94}As$ films grown on both the nominally flat substrate and misoriented GaAs(001) substrate, where $\mathbf{E}_{\perp}$ and $\mathbf{E}_{||}$ refer to electric field vector **E** perpendicular and parallel to [110].

strain relaxation symmetry determined by XRC.

In order to study in detail the local variations in strain, we performed CLWI and LPCL imaging on both these samples. In CLWI imaging the wavelength, λ_m, at which the intensity of luminescence is a maximum is mapped as a function of the spatial (x,y) position, and a gray-scale image representing these wavelengths is generated. A scanning area of 128×94 μm^2 in this study is discretized into 640×480 pixels. In order to determine $\lambda_m(x,y)$, a spectrum consisting of 29 wavelength points (obtained from 29 discrete monochromatic CL images), varying from 860 to 874 nm (1441 to 1418 meV), was obtained at each pixel position.

The CLWI, the LPCL, and the spectrally integrated (i.e., panchromatic for the $860\leq\lambda\leq874$ nm range) images were taken over the same 128×94 μm^2 regions in both nominally flat and misoriented samples. The spectrally integrated images allow identification of nonradiative recombination centers associated with defects. The CLWI micrographs of the nominally flat and misoriented samples are shown in Figs. 3(a) and 4(a), respectively. The mapping of λ_m into a gray-scale representation is

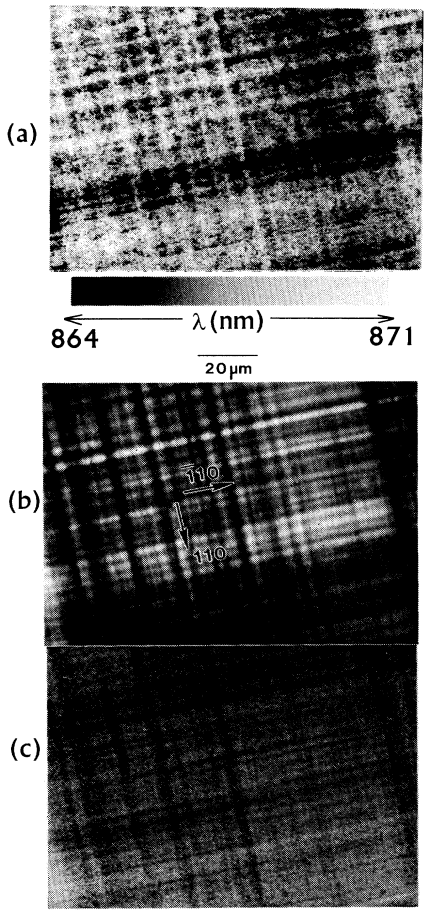

FIG. 3. The CLWI, the integrated CL intensity, and the LPCL images in (a), (b), and (c), respectively, for the $In_{0.06}Ga_{0.94}As$ film grown on the flat substrate. A scale showing the mapping of wavelengths of peak CL intensity is shown in (a).

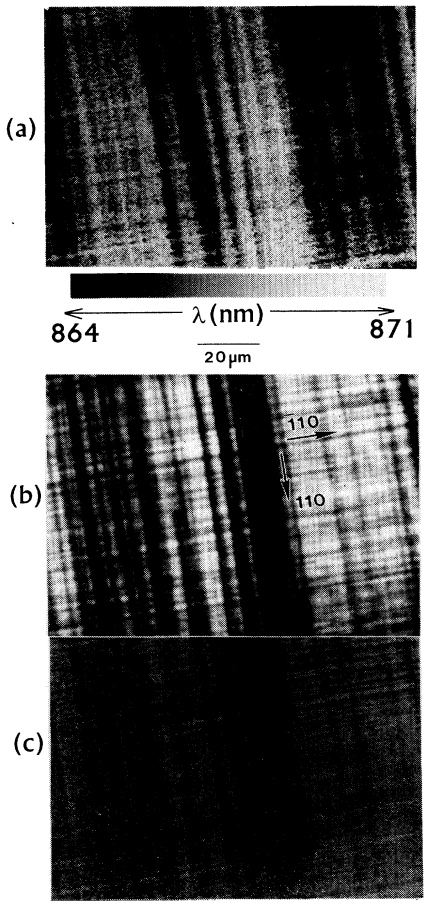

FIG. 4. The CLWI, the integrated CL intensity, and the LPCL images in (a), (b), and (c), respectively, for the $In_{0.06}Ga_{0.94}As$ film grown on the misoriented substrate. A scale showing the mapping of wavelengths of peak CL intensity is shown in (a).

shown by the gray-bar key indicating the wavelength scale. Figures 3(b) and 4(b) show integrated CL intensity micrographs. Long streaks of a constant gray shade can be seen in Figs. 3(a) and 4(a), which correlate in position and orientation with the DLD's in the integrated CL intensity images. These DLD's have been observed previously in CL imaging of partially relaxed $In_xGa_{1-x}As$ films grown on GaAs.[10,11] The reduction in the luminescence effect is due to the presence of nonradiative recombination centers, likely caused by the presence of misfit dislocation cores and point defects left in the wake of dislocation propagation.[10]

Figures 3(c) and 4(c) show monochromatic LPCL images for the samples grown on the flat and misoriented substrates, respectively. Images were taken with the polarizer rotated to detect emission of light with $\mathbf{E}_\perp[110]$ and $\mathbf{E}_\parallel[110]$ detection orientations at a wavelength of 869 nm (1426 meV). In order to emphasize the polarization variations, the ratio of these images is displayed in Figs. 3(c) and 4(c). The pixels in the ratio image at a (x,y) position are represented as $\log_{10}[I_\perp(x,y)/I_\parallel(x,y)]$, where $I_\perp$ and $I_\parallel$ are the pixel intensities under $\mathbf{E}_\perp[110]$ and $\mathbf{E}\parallel[110]$ detection orientations, normalized to a 256 level gray scale. The bright and the dark bands present in the LPCL ratio images clearly exhibit the local polarization anisotropy, which indicates the presence of μm-scale variations in strain. A distinct asymmetry in the CLWI, spectrally integrated, and LPCL images is observed in Fig. 4 for the misoriented substrate, in which a greater density of DLD, constant-wavelength and polarization-ratio streaks is observed along the [110] direction. This asymmetry is markedly reduced in Fig. 3 for the flat substrate, consistent with the XRC results.

Figure 5 shows the correlation existing between the CLWI image, the integrated CL image, and the LPCL images for the misoriented substrate. The results for the flat substrate are qualitatively similar, and are not shown here. Peak wavelength (λ_m), luminescence intensity and $I_\perp/I_\parallel$ ratios are plotted as a function of the distance taken along an arbitrary [1$\bar{1}$0]-oriented line. The histogram shows that the blueshifted and the redshifted regions correspond to the regions of enhanced and reduced luminescence efficiency [bright and dark regions in Figs. 3(b) and 4(b)]. Regions of reduced luminescence efficiency are due to an enhanced nonradiative recombination near misfit dislocation cores. The material has also relaxed in the regions near the dislocations, resulting in a change in the band gap, i.e., a reduction in the compressive stress has resulted in a redshift seen in the CLWI imaging. In the regions of enhanced luminescence, where there are very few dislocations, little relaxation has occurred, resulting in a higher biaxial compressive stress, which gives rise to a relative blueshift.

Our hypothesis that the blueshift and redshift seen in CLWI imaging is due to variation in strain and not due to alloy variation, is supported by the correlation between the CLWI and LPCL images, as evident from the histogram analysis. In Fig. 5, the histograms show that regions of enhanced and reduced luminescence efficiency correspond to regions of reduced and enhanced polarization anisotropy, and also correspond to regions of blue-

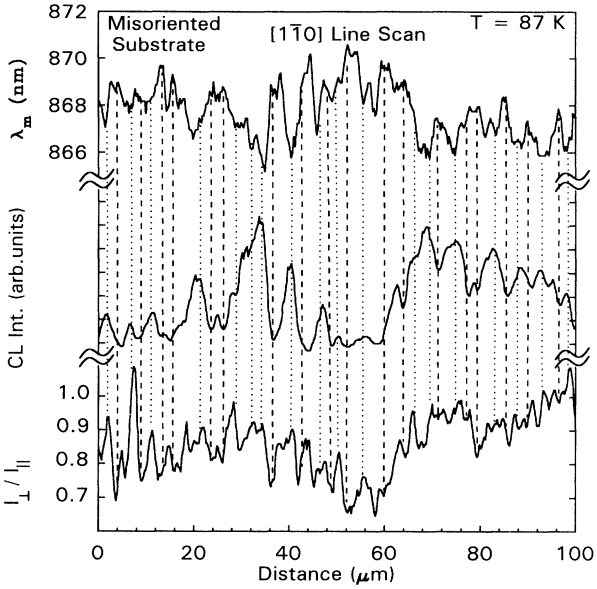

FIG. 5. Histogram of CLWI, integrated CL intensity and LPCL $I_\perp/I_\parallel$ ratio for an arbitrary line scan done along the [1$\bar{1}$0] for the sample grown on the misoriented substrate. The spatial correlation of the regions showing redshift, a decreased luminescence efficiency, and enhanced polarization (indicated by dashed vertical lines) and regions with a blueshift, increased luminescence efficiency and no polarization (indicated by dotted vertical lines) is observed.

shift and redshift in the CLWI image, respectively. In the regions of high misfit dislocation density, i.e., reduced luminescence efficiency, the material is preferably relaxed in a direction perpendicular to the dislocation line direction, resulting in a deviation from an ideal biaxial stress with $\sigma_\parallel = \sigma_\perp$, and this causes a polarization anisotropy ($I_\perp/I_\parallel < 1$). In the regions of low dislocation density (high luminescence efficiency) very little relaxation has occurred, thus resulting in minimal deviation from biaxial stress with $I_\perp/I_\parallel \approx 1$. Regions which show an enhanced polarization anisotropy correspond to regions which exhibit a redshift in the CLWI images. This further indicates that a local reduction in stress occurs along [1$\bar{1}$0], which leads to a [110]-oriented quasiuniaxial stress that is consistent with the lh polarization selection rules previously discussed.

The minimum polarization ratios ($I_\perp/I_\parallel$) are, however, greater than the theoretical value of 0.29 for pure uniaxial stress, as shown in Fig. 1. This is explained with the help of a model where the strain component perpendicular to the DLD's is not completely relaxed and a quasiuniaxial stress with a dominant longitudinal component, $\sigma_\parallel$, parallel to the DLD's is present such that $\sigma_\parallel \gg \sigma_\perp$. The presence of a quasiuniaxial stress as opposed to a pure uniaxial stress ($\sigma_\perp = 0$) results in a considerable mixing of the hh and lh characters in the strain-split band (see Fig. 1), which causes the polarization ratios to deviate from theoretically predicted values for $\sigma_\perp = 0$.

V. SUMMARY AND CONCLUSIONS

In conclusion, we have studied extensively the distribution of dark line defects associated with misfit dislocations using CLWI and LPCL. We have shown the existence of local variations in compressive stress ranging from biaxial with $\sigma_{\parallel} \approx \sigma_{\perp}$ to quasiuniaxial with $\sigma_{\parallel} \gg \sigma_{\perp}$, resulting in a marked polarization anisotropy concomitant with a variation in luminescence transition energy. The effect of substrate misorientation has been examined, and $In_xGa_{1-x}As$ growth on misoriented substrates results in a greater anisotropy in strain relaxation and polarization of excitonic luminescence. These results show that dark line defects in strained systems exhibit significant polarization and energy variations in addition to their more familiar nonradiative behavior.

ACKNOWLEDGMENTS

This work was supported by the Charles Lee Powell Foundation, NSF(PYI-DMR), NSF(RIA-ECS), ONR, and the Army Research Office.

---

*Author to whom correspondence should be addressed.

[1]G. H. Olsen, M. S. Abrahams, and T. J. Zamerowski, J. Electrochem. Soc. **121**, 1650 (1974).

[2]E. A. Fitzgerald, D. G. Ast, P. D. Kirchner, G. D. Petit, and J. M. Woodall, J. Appl. Phys. **63**, 693 (1988).

[3]K. L. Kavanagh, M. A. Capano, L. W. Hobbs, J. C. Barbour, P. M. J. Maree, W. Schaff, J. W. Mayer, G. D. Petit, J. A. Stroscio, and R. M. Feenstra, J. Appl. Phys. **64**, 4843 (1988).

[4]B. A. Fox and W. A. Jesser, J. Appl. Phys. **68**, 2739 (1990).

[5]M. Grundmann, U. Liener, D. Bimberg, A. Fischer-Colbrie, and J. N. Miller, Appl. Phys. Lett. **55**, 1765 (1989).

[6]J. J. Duga, J. Appl. Phys. **33**, 169 (1962).

[7]J. Chen, J. M. Fernandez, and H. H. Wieder, in *Mechanisms of Heteroepitaxial Growth,* edited by M.F. Chisholm, R. Hull, L.J. Schowalter, and E.J. Garrison, MRS Symposia Proceedings No. 263 (Materials Research Society, Pittsburgh, 1992), p. 377.

[8]T. Schweizer, K. Kohler, W. Rothemund, and P. Ganser, Appl. Phys. Lett. **59**, 2736 (1991).

[9]D. Morris, Q. Sun, C. Lacelle, A. P. Roth, J. L. Brebner, M. Simard-Normandin, and K. Rajan, J. Appl. Phys. **71**, 2321 (1992).

[10]D. H. Rich, T. George, W. T. Pike, J. Maserjian, F. J. Grunthaner, and A. Larsson, J. Appl. Phys. **72**, 5834 (1992).

[11]E. A. Fitzgerald, G. P. Watson, R. E. Proano, D. G. Ast, P. D. Kirchner, G. D. Petit, and J. M. Woodall, J. Appl. Phys. **65**, 2220 (1989).

[12]R. S. Goldman, H. H. Wieder, K. L. Kavanagh, K. Rammohan, and D. H. Rich, Appl. Phys. Lett. **65**, 1424 (1994); R. S. Goldman, K. Rammohan, A. Raisanen, M. Goorsky, L. J. Brillson, D. H. Rich, H. H. Wieder, and K. L. Kavanagh (unpublished).

[13]Y. Chen, N. D. Zakharaov, P. Werner, Z. Liliental-Weber, J. Washburn, J. F. Klem, and J. Y. Tsao, Appl. Phys. Lett. **62**, 1536 (1993).

[14]D. H. Rich, A. Ksendzov, R. W. Terhune, F. J. Grunthaner, B. A. Wilson, H. Shen, M. Dutta, S. M. Vernon, and T. M. Dixon, Phys. Rev. B **43**, 6836 (1991).

[15]Y. Tang, D. H. Rich, E. H. Lingunis, and N. M. Haegel, J. Appl. Phys. **76**, 3032 (1994).

[16]M. Grundmann, J. Christen, D. Bimberg, A. Hashimoto, T. Fukunaga, and N. Watanabe, Appl. Phys. Lett. **58**, 2090 (1991).

[17]F. H. Pollak and M. Cardona, Phys. Rev. **172**, 816 (1968).

[18]S. Adachi, J. Appl. Phys. **53**, 8775 (1982).

[19]S. Niki, C. L. Lin, S. C. Chang, and H. H. Wieder, Appl. Phys. Lett. **55**, 1339 (1989).

[20]V. Swaminathan and A. T. Macrander, *Materials Aspects of GaAs and InP Based Structures* (Prentice-Hall, Englewood Cliffs, NJ, 1991), pp. 21–25.

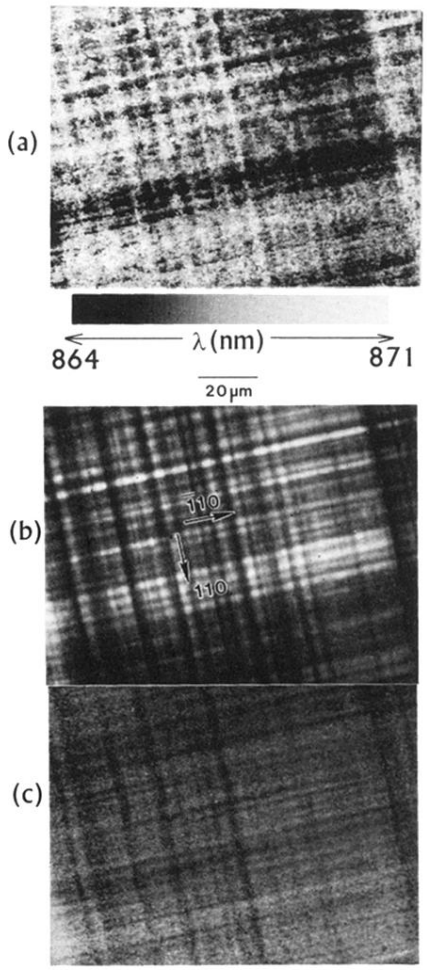

FIG. 3. The CLWI, the integrated CL intensity, and the LPCL images in (a), (b), and (c), respectively, for the $In_{0.06}Ga_{0.94}As$ film grown on the flat substrate. A scale showing the mapping of wavelengths of peak CL intensity is shown in (a).

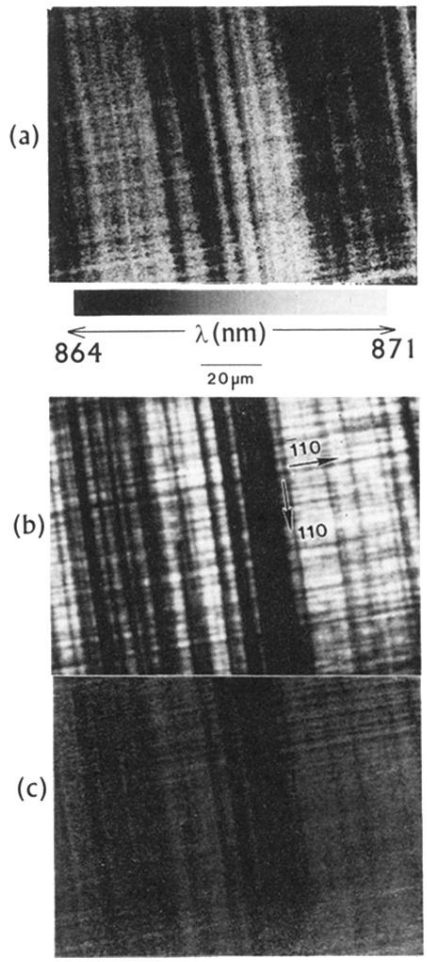

FIG. 4. The CLWI, the integrated CL intensity, and the LPCL images in (a), (b), and (c), respectively, for the $In_{0.06}Ga_{0.94}As$ film grown on the misoriented substrate. A scale showing the mapping of wavelengths of peak CL intensity is shown in (a).